

RSC Advances



This article can be cited before page numbers have been issued, to do this please use: Z. Sun, D. Guo, H. Li, L. Zhang, B. Yang and S. Yan, *RSC Adv.*, 2015, DOI: 10.1039/C4RA13487G.



This is an *Accepted Manuscript*, which has been through the Royal Society of Chemistry peer review process and has been accepted for publication.

Accepted Manuscripts are published online shortly after acceptance, before technical editing, formatting and proof reading. Using this free service, authors can make their results available to the community, in citable form, before we publish the edited article. This *Accepted Manuscript* will be replaced by the edited, formatted and paginated article as soon as this is available.

You can find more information about *Accepted Manuscripts* in the [Information for Authors](#).

Please note that technical editing may introduce minor changes to the text and/or graphics, which may alter content. The journal's standard [Terms & Conditions](#) and the [Ethical guidelines](#) still apply. In no event shall the Royal Society of Chemistry be held responsible for any errors or omissions in this *Accepted Manuscript* or any consequences arising from the use of any information it contains.

ARTICLE

Multifunctional Fe₃O₄@SiO₂ nanoparticles for selective detection and removal of Hg²⁺ ion in aqueous solution

Cite this: DOI: 10.1039/x0xx00000x

Zebin Sun,^a Dan Guo,^a Haizhen Li,^a Li Zhang,^a Bo Yang^a and Shiqiang Yan*^aReceived 00th January 2012,
Accepted 00th January 2012

DOI: 10.1039/x0xx00000x

www.rsc.org/

In the present work, a multifunctional magnetic core-shell Fe₃O₄@SiO₂ nanoparticle decorated with rhodamine-based receptor, which exhibits high selectivity and sensitivity toward Hg²⁺ over other metal ions in aqueous solution, has been synthesized by the graft method and characterized by transmission electron microscopy, Fourier transform infrared spectroscopy, X-ray diffraction, vibrating sample magnetometry, and UV-vis absorption and fluorescence spectra. The multifunctional nanoparticles show superparamagnetic behavior, clear core-shell architecture, and also exhibit high optical sensing performance for the detection of Hg²⁺. The fluorogenical responses of RB-Fe₃O₄@SiO₂ are stable under a broad pH range. Additionally, these nanoparticles show high performance in the magnetic separability and effective removal of excess Hg²⁺ in water via an external magnetic field. These results indicate that these multifunctional magnetic nanoparticles may find potential and practical applications for selective detection and simple removal of Hg²⁺ in environmental, toxicological, and biological fields.

1. Introduction

In recent years, considerable effects have been devoted to the development of optical sensors that can selectively detect and signal toxic heavy metal ions because of the wide use of these metal ions and their potential implications in environmental and biological fields.¹⁻⁵ Of these ions, mercury is one of the most dangerous and hazardous heavy metal elements and has a significant impact on the public health. Recent investigations revealed that mercury can lead to the dysfunction of cells and many health problems in kidney, brain, and central nervous system owing to its high affinity for thiol group in enzymes and proteins.⁶⁻⁸ Therefore, it is still highly desirable to develop new fluorescence chemosensors for the selective detection of Hg²⁺ and the removal of excessive of Hg²⁺ in environmental and biological samples.

Optical chemosensors have recently attracted great attention via exhibiting virtues of fast, easy, and non-destructive sensing, and inexpensive and simple detection procedures compared with traditional determination techniques.⁹⁻¹⁴ Recently, some small molecule fluorescent probes have been reported for the detection of Hg²⁺ with excellent detection properties.¹⁵⁻²⁶ However, most of the previous organic fluorescent sensors suffered from some drawbacks. For example, the sensing molecules are difficult to dissolve in aqueous media and can't work in pure water.^{27, 28} Additionally, the traditional organic chemosensors show the fluorescence emission quenching²⁹⁻³³ and poor performance for the removal of Hg²⁺ from the heterogeneous solid-liquid phase. Hence, the development of sensing probes that can selectively detect and remove excessive Hg²⁺ in heterogeneous system with fluorescence enhancement is still highly expected.

It is well known that rhodamine derivatives are valuable platform for selective detection of metal ions leading to strongly fluorescent colorful open ring structure.³⁴⁻⁴⁰ Rhodamine-based dyes are utilized extensively as highly

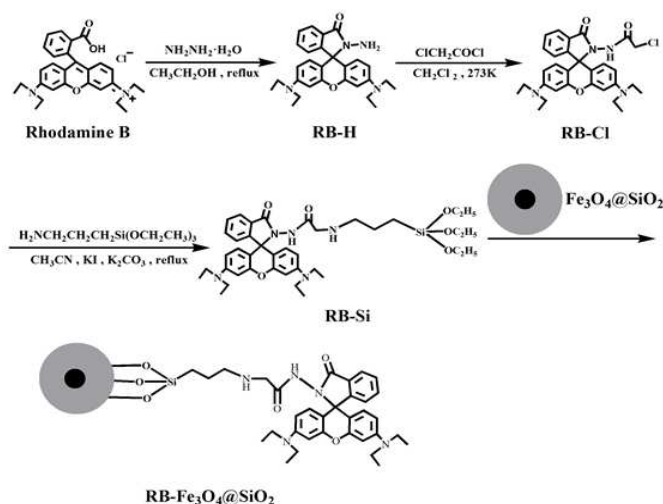
selective and sensitive chemosensors for ionic species owing to their high absorption coefficient, high fluorescence quantum yields, long absorption and emission wavelength, and the possibility of naked-eye detection.^{25, 35}

Recently, the organic-inorganic hybrid nanoparticles have been utilized extensively as sensing probes with high selectivity and sensitivity. The receptor-immobilized inorganic nanomaterials, including SiO₂,⁴¹⁻⁴³ MCM-41,^{44, 45} SBA-15,⁴⁶⁻⁴⁸ MCM-48,⁴⁹ Fe₃O₄,^{50, 51} and Fe₃O₄@SiO₂,⁵² have some significant advantages over some organic molecule probes which are difficult to dissolve in aqueous solution and they can simply and effectively detect some targets in heterogeneous solid-liquid phase.⁴² The recent study revealed that magnetic core-shell Fe₃O₄@SiO₂ nanoparticles can be widely applied in biological and environmental fields. As an inorganic carrier, magnetic core-shell Fe₃O₄@SiO₂ has some significant advantages.^{53, 54} For example, the magnetic Fe₃O₄ nanoparticles in Fe₃O₄@SiO₂ nanoparticles can facilitate magnetic separation from the detection system via an external magnetic field. Furthermore, the inner silica shell of Fe₃O₄@SiO₂ nanoparticles can prevent their aggregation in solution, improve the chemical stability of nanoparticles and provide better protection against toxicity.^{55, 56} In addition, the silica shell coating on the surface of Fe₃O₄@SiO₂ nanoparticles can also provide many sites for surface modification with organic small molecule probes owing to their large specific surface area. However, magnetic core-shell nanoparticles, which can separate and remove toxic environmental pollutants in aqueous solution, are very rare.

Bearing the above statement in mind, we synthesized an inorganic-organic hybrid nanoparticle by immobilizing rhodamine-based receptor onto the silica nanoshell of Fe₃O₄@SiO₂ nanoparticles as a convenient approach for selective detection and effective removal of Hg²⁺ ions. The well-designed magnetic core-shell nanoparticle shows high selectivity toward Hg²⁺ in the presence of various coexisting

ARTICLE

ionic species in aqueous solution with a detection limit of 2.13×10^{-6} M. Furthermore, **RB-Fe₃O₄@SiO₂** can also effectively remove excess Hg²⁺ from the aqueous solution with an external magnetic field.



Scheme 1. Synthetic procedure of **RB-Fe₃O₄@SiO₂**.

2. Experimental

2.1 Materials and Characterization

Rhodamine B, tetraethoxysilane (TEOS), hydrazine hydrate (85%), 3-aminopropyltriethoxysilane (APTES), chloroacetyl chloride, mercury nitrate and other nitrate salts of metal ion (K⁺, Na⁺, Ag⁺, Mg²⁺, Ca²⁺, Ba²⁺, Co²⁺, Ni²⁺, Cu²⁺, Zn²⁺, Cd²⁺, Pb²⁺), and other reagents were commercially bought from Tianjin Chemical Company (Tianjin, China) and used without further purifications.

¹H NMR spectra was recorded using Varian mercury-400 spectrometer with TMS as an internal standard and DMSO as solvent. Mass spectra were determined on a Bruker Daltonics-esquire 6000 mass spectrometer. Transmission electron microscopy (TEM, TecnaiG²F30, FEI, USA) and dynamic light scattering (BI-200SM, Brookhaven Instruments Corporation, Holtsville, NY, USA) were used to characterize the materials. Fourier transform infrared (FTIR) spectra were recorded on a NEXUS 670 FTIR spectrometer (Nicolet Instrument Corporation, USA) using KBr discs in the 400–4000 cm⁻¹ region. X-ray powder diffraction (XRD) patterns of all samples were analyzed with an X'Pert Pro Philips X-ray diffractometer with Cu-Kα radiation, and the scan range (2θ) was from 10° to 80°. Magnetic properties were determined by a vibrating sample magnetometry (VSM, LAKESHORE-7304) at 300 K. Thermal gravimetric analysis (TGA, Dupont 1090B, Dupont, USA) was performed at a heating rate of 10 °C min⁻¹ and a nitrogen flow of 10 mL min⁻¹. The concentration of Hg²⁺ remaining in aqueous solution was detected by using an inductively coupled plasma spectrometer (ICP-OES, Varian, USA). Absorption spectra were performed on a Varian UV-Cary 100 spectrophotometer. Fluorescence spectra measurements were determined on a Hitachi F-4500 fluorescence spectrofluorimeter. All pH values were measured on PHS-3C digital pH meter (Shanghai, China).

2.2 Preparation of Fe₃O₄@SiO₂

The magnetic nanoparticles were synthesized by a similar method developed by Haynes et al.⁵⁷ Under N₂ atmosphere, FeCl₃·6H₂O (4.8 g, 17.81 mmol), FeCl₂·4H₂O (2.00 g, 10.02 mmol) and 0.85 mL oleic acid were added to 30 mL of deionized water with vigorous stirring. The reaction mixture solution was heated to 90 °C. Then, about 20 mL of ammonium hydroxide (14 wt%) was subsequently added rapidly to the mixture solution, and the mixture was kept at 90 °C for 2.5 h. The mixture solution was then allowed to cool to room temperature. The synthesized Fe₃O₄ nanoparticles was collected and resuspended in chloroform with a concentration of 54.5 mg mL⁻¹ oleic acid-capped Fe₃O₄.

About 10 mg of oleic acid-capped Fe₃O₄ nanoparticles were added to 30 mL of cyclohexane at room temperature. Then Triton X-100 (5.4 g), hexane (4.8 mL) and H₂O (1 mL) were added with stirring to form a water-in-oil microemulsion. After 15 min, 0.4 mL of TEOS was added slowly to the reaction solution with vigorous stirring. After 1.5 h, 1 mL of aqueous ammonia (28–30 wt%) was added to the mixture, the reaction was kept for another 24 h to form the Fe₃O₄@SiO₂ nanoparticles. The Fe₃O₄@SiO₂ nanoparticles were isolated via centrifugation and washed with ethanol five times and deionized water five times to remove adherent surfactant and unreacted chemicals.

2.3 Synthesis of rhodamine B hydrazide (RB-H)

RB-H was prepared according to the published procedure.⁵⁸

2.4 Synthesis of RB-Cl

A solution of RB-H (0.456 g, 1.0 mmol) in dry dichloromethane (30 mL) was cooled with ice bath. Then chloroacetyl chloride (0.17 g, 1.5 mmol) was dissolved in 5 mL dichloromethane and added dropwise to the solution with vigorous stirring. After the addition, the ice bath was kept for about 2 h under nitrogen atmosphere. After the solvent was evaporated under reduced pressure, the crude product was purified by column chromatography (petroleum ether/ethyl acetate, 2:1, v/v) to give the 0.4578 g of RB-Cl as a white solid (yield, 86%). ¹H NMR (400 MHz, DMSO, ppm) (Fig. S1), δ: 1.08 (12H, t, J = 6.9 Hz), 3.25–3.35 (8H, m), 3.99 (2H, s), 6.33 (4H, d, J = 7.7 Hz), 6.50 (2H, d, J = 9.2 Hz), 7.02 (1H, d, J = 7.7 Hz), 7.50–7.59 (2H, m), 7.83 (1H, d, J = 7.0 Hz), 9.93 (1H, s). ESI-MS (m/z) (Fig. S2): 533.2154 (M + H)⁺.

2.5 Synthesis of RB-Fe₃O₄@SiO₂

Alkoxysilane modified RB-Si was synthesized by using the procedure described in literature.⁵² A mixture of 3-aminopropyltriethoxysilane (88.4 mg, 0.4 mmol), RB-Cl (0.213 g, 0.4 mmol), K₂CO₃ (55.2 mg, 0.6 mmol), KI (5 mg, 0.03 mmol) and acetonitrile (30 mL) was heated to 80 °C for 10 h under N₂ atmosphere and then cooled down to room temperature. After filtration of salts, the filtrate was evaporated under reduced pressure. Then the product was purified by column chromatography (ethyl acetate) to give RB-Si: ¹H NMR (400 MHz, DMSO, ppm) (Fig. S3), δ: 0.46 (2H, m), 1.07–1.15 (21H, m), 1.41 (2H, m), 2.38 (2H, m), 3.29–3.33 (10H, m), 3.73 (6H, m), 6.34 (4H, d, J = 9.6 Hz), 6.52 (2H, d, J = 8.5 Hz), 7.03 (1H, d, J = 7.0 Hz), 7.56 (2H, dd, J = 7.5, 6.4 Hz), 7.85 (1H, d, J = 6.7 Hz). IR: –C–NH 3445.0 cm⁻¹, –(CH₂)₃– 2971.6, 2927.6, 2887.6 cm⁻¹; Si–O 1076.7, 786.6 cm⁻¹. Then the hybrid material of **RB-Fe₃O₄@SiO₂** was prepared as follows: RB-Si (200 mg) and Fe₃O₄@SiO₂ (200 mg) were suspended in anhydrous toluene (40 mL) and stirred under nitrogen atmosphere for 24 h. Then the resulting products were

isolated by centrifugation, and repeatedly washed with toluene, dichloromethane, and ethanol several times under ultrasonic condition. The product was dried under vacuum for 12 h.

3. Results and discussion

3.1 Material characterizations

To ascertain the presence of organic ligands on the surface of **RB-Fe₃O₄@SiO₂**, the FT-IR spectra of RB-Cl (a), RB-Si (b), and **RB-Fe₃O₄@SiO₂** (c) are shown in Fig. 1 for comparison. The absorption band at 3445.0 cm⁻¹ in Fig. 1b is attributed to the strong vibration of NH. The emergence of a series of bands at 2971.6, 2927.6, 2887.6 cm⁻¹ in Fig. 1b is attributed to the vibration of methylene $-(\text{CH}_2)_3-$. Furthermore, the spectra of RB-Si in Fig. 1b is dominated by ν_{as} (Si-O, 1076.7 cm⁻¹), ν_{s} (Si-O, 786.6 cm⁻¹) absorption bands, exhibiting the characteristic absorption peaks of trialkoxysilyl functions. It is thus proved that RB-Si has been successfully synthesized.⁵⁹ The FT-IR spectrum of **RB-Fe₃O₄@SiO₂** (Fig. 1c) shows new and strong absorption peaks at 1096.1 cm⁻¹ (ν_{as} , Si-O), 797.1 cm⁻¹ (ν_{s} , Si-O), and 468.0 cm⁻¹ (δ , Si-O-Si) (ν represents stretching, δ in plane bending, s symmetric, and as asymmetric vibrations), suggesting the formation of Si-O-Si framework. Hence, based on the above results, it is proved that the organic ligands (RB-Si) are immobilized onto the surface of **RB-Fe₃O₄@SiO₂**.⁶⁰

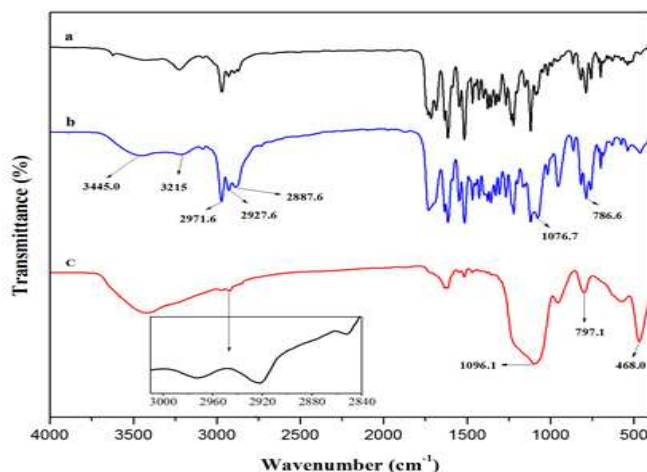


Fig. 1. FT-IR spectra for RB-Cl (a), RB-Si (b), and **RB-Fe₃O₄@SiO₂** (c).

Fig. 2 shows the X-ray powder diffraction patterns of Fe₃O₄@SiO₂ nanoparticles (a) and **RB-Fe₃O₄@SiO₂** nanocomposites (b). As can be observed, both samples show the characteristic diffraction peaks at (220), (311), (400), (511), and (440), which agree well with the data for pure cubic Fe₃O₄, as reported in the JCPDS card (No. 88-315, a = 8.375).⁶¹ The broad feature peak at 20 - 28° in Fig. 2 corresponds to the silica, which reveals that the silica shell is successfully coated on the surface of the magnetic nanoparticles. The XRD patterns of the **RB-Fe₃O₄@SiO₂** nanocomposites are the same as that of Fe₃O₄@SiO₂ nanoparticles, suggesting that the organically modified procedure does not cause the phase changes of Fe₃O₄@SiO₂ nanoparticles.

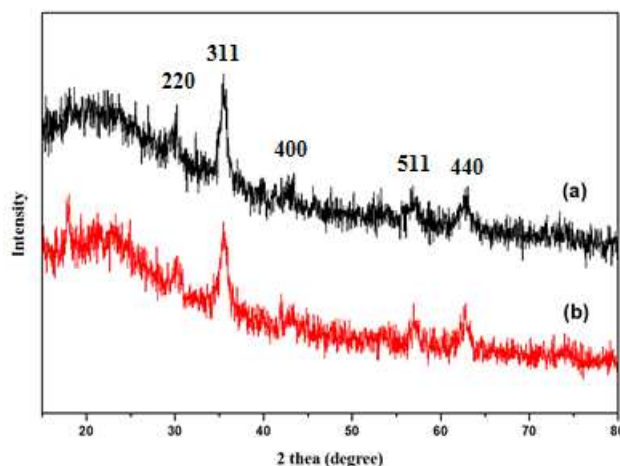


Fig. 2. XRD patterns of Fe₃O₄@SiO₂ (a) and **RB-Fe₃O₄@SiO₂** (b).

The TEM images of Fe₃O₄@SiO₂ (a) and **RB-Fe₃O₄@SiO₂** (b) are shown in Fig. 3. It can be seen that these nanoparticles have clear core shell structure, and the spherical shape of the nanoparticles is observed. It also can be observed that iron oxide nanoparticles had been trapped in the silica shell successfully, in which an average particle diameter is about 50-60 nm with about 10 nm Fe₃O₄ core. The thickness of the silica shell of these nanoparticles is uniform and the surface of the silica shell seems to be quite smooth. In addition, dynamic light scattering (DLS) was performed to further reveal the stability of the core-shell particles in the aqueous state. According to the DLS results (Fig. S4), **RB-Fe₃O₄@SiO₂** presents good stabilization and has an average size of 167 nm, confirming its good stabilization in the aqueous state. In a common sense, the particles diameter difference between TEM and DLS measurements is attributed to the hydrodynamic radius and the grafted molecule.^{54, 62-64} Hence, these results reveal that the core-shell particles have good stabilization in the aqueous state, which is useful for practical applications.

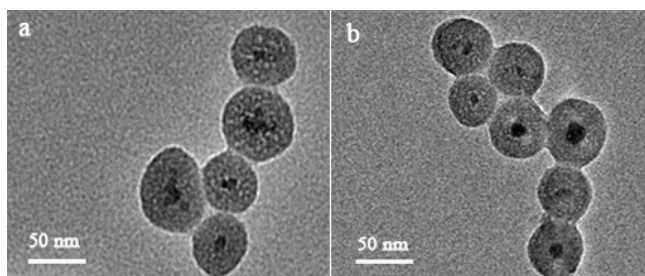


Fig. 3. TEM images of Fe₃O₄@SiO₂ (a) and **RB-Fe₃O₄@SiO₂** (b).

The TGA measurement for Fe₃O₄@SiO₂ (a) and **RB-Fe₃O₄@SiO₂** (b) are presented in Fig. 4, which are performed on a Dupont-1090 thermogravimeter in N₂ atmosphere at a heating rate of 10 °C min⁻¹ and a nitrogen flow of 10 mL min⁻¹ from 50 to 650 °C. As shown in Fig. 4a, the Fe₃O₄@SiO₂ nanoparticles show a weight loss of about 4.0% between 50 and 650 °C corresponding to the desorption of physically adsorbed water from the surface of the silica layer and the loss of the structure water.⁶⁵ From the TGA weight loss curve of **RB-Fe₃O₄@SiO₂** in Fig. 4, the TGA curve presents two main steps of thermal decomposition between 50-327.9 °C and

327.9-650 °C, respectively. As for the two steps, there is a total weight loss of 14.10%, which is mainly attributed to two water loss events and the thermal degradation of the organic moiety immobilized on the surface of $\text{Fe}_3\text{O}_4@\text{SiO}_2$. Therefore, comparing with Fig. 4a, we determine that the quantity of the organic dye attached to the surface of $\text{Fe}_3\text{O}_4@\text{SiO}_2$ is about 10.10%.

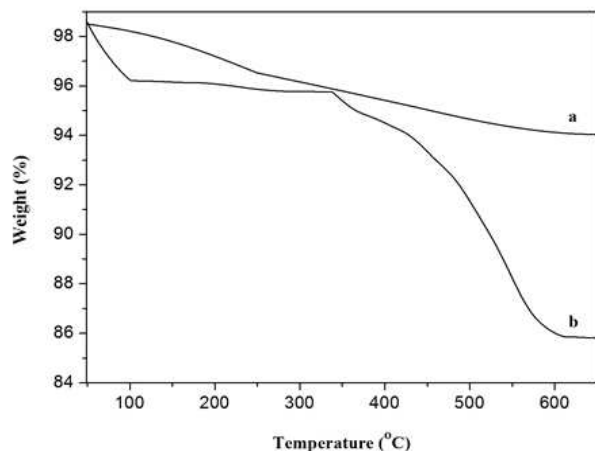


Fig. 4. TGA curves of $\text{Fe}_3\text{O}_4@\text{SiO}_2$ (a) and $\text{RB-Fe}_3\text{O}_4@\text{SiO}_2$ (b).

The magnetic characterizations of $\text{Fe}_3\text{O}_4@\text{SiO}_2$ (a) and $\text{RB-Fe}_3\text{O}_4@\text{SiO}_2$ (b) were achieved using a vibrating sample magnetometer at 300 K (Fig. 5). The saturation magnetization values are 19.3 emu g^{-1} and 7.78 emu g^{-1} for $\text{Fe}_3\text{O}_4@\text{SiO}_2$ and $\text{RB-Fe}_3\text{O}_4@\text{SiO}_2$, respectively. In addition, the magnetization curves of both samples exhibit no hysteresis loops. Neither coercivity nor remanence is observed for all of the samples, which suggest that both nanoparticles are superparamagnetic.⁶⁵ Fig. 5 inset shows the separation process of $\text{RB-Fe}_3\text{O}_4@\text{SiO}_2$ in water. As can be observed, when a magnet was placed near the vial, materials were quickly separated within a few minutes, suggesting the $\text{RB-Fe}_3\text{O}_4@\text{SiO}_2$ can be easily separated from the solution system by adding an external magnetic field.

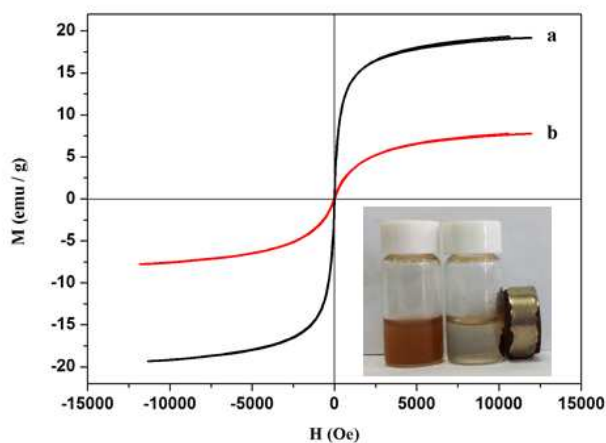


Fig. 5. Magnetic curves of $\text{Fe}_3\text{O}_4@\text{SiO}_2$ (a) and $\text{RB-Fe}_3\text{O}_4@\text{SiO}_2$ (b). (Inset: Photographs of the separation process of $\text{RB-Fe}_3\text{O}_4@\text{SiO}_2$ in aqueous solution).

3.2 Absorption spectroscopy studies

The UV-vis titration absorption spectra of $\text{RB-Fe}_3\text{O}_4@\text{SiO}_2$ in aqueous solution are provided in Fig. 6. The $\text{RB-Fe}_3\text{O}_4@\text{SiO}_2$ sensor shows a weak absorption in the above 500 nm in the absence of Hg^{2+} , which can be ascribed to the fact that $\text{RB-Fe}_3\text{O}_4@\text{SiO}_2$ exists as a close ring spirolactam form in solution. Upon addition of Hg^{2+} , the solution of $\text{RB-Fe}_3\text{O}_4@\text{SiO}_2$ turned from colorless to red (Fig. 6, inset). A new absorption centered at 570 nm appeared and was enhanced by the addition of increasing concentration of Hg^{2+} ions, suggesting that the open ring structure of $\text{RB-Fe}_3\text{O}_4@\text{SiO}_2$ is due to the Hg^{2+} binding. Such a distinct color change shows that the $\text{RB-Fe}_3\text{O}_4@\text{SiO}_2$ can be utilized as selective “naked-eye” sensor for Hg^{2+} . It was significant to ascertain the selectivity of $\text{RB-Fe}_3\text{O}_4@\text{SiO}_2$ for which nitrate salts of Na^+ , K^+ , Ba^{2+} , Mg^{2+} , Ca^{2+} , Zn^{2+} , Cd^{2+} , Cu^{2+} , Co^{2+} , Ni^{2+} , Pb^{2+} , Hg^{2+} , and Ag^+ in aqueous solution were selected. As shown in Fig. 7a, an obvious change in UV-vis spectral pattern was manifested in presence of Hg^{2+} , while other metal ions failed to lead to any conspicuous absorption change in the visible range except there was relatively smaller ultraviolet absorption enhancement with Cu^{2+} . Among these metal ions, only Hg^{2+} and Cu^{2+} exhibit distinct detectable color changes, whereas other competitive cations did not reveal any significant changes under identical conditions, as shown in Fig. 7b. Moreover, the competitive experiment also revealed that the coexisting metal ions exhibited low interference with the detection of Hg^{2+} in aqueous solution (Fig. 8). These results indicated that the “naked-eye” detection of Hg^{2+} by $\text{RB-Fe}_3\text{O}_4@\text{SiO}_2$ is not significantly influenced by other competitive metal ions and hence $\text{RB-Fe}_3\text{O}_4@\text{SiO}_2$ shows a high selectivity toward Hg^{2+} in water.

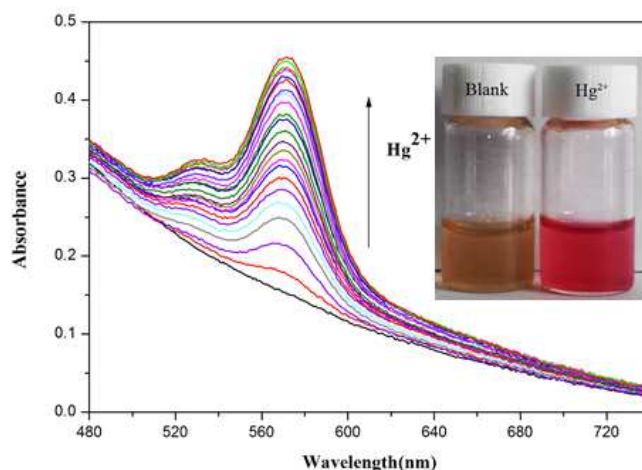


Fig. 6. Absorption spectra of $\text{RB-Fe}_3\text{O}_4@\text{SiO}_2$ (0.3 mg/mL) in aqueous solution upon addition of various amounts of Hg^{2+} ($0-6.0 \times 10^{-4} \text{ M}$). Inset shows the distinct naked eye color change of $\text{RB-Fe}_3\text{O}_4@\text{SiO}_2$ (0.3 mg/mL) upon addition of Hg^{2+} ($6.0 \times 10^{-4} \text{ M}$).

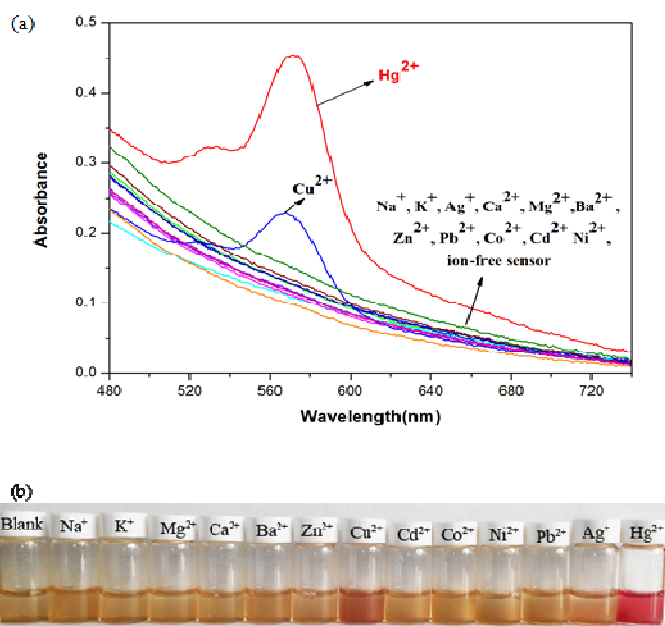


Fig. 7. (a) Absorption spectra of **RB-Fe₃O₄@SiO₂** (0.3 mg/mL) in aqueous solution upon addition of various metal ions (all are 6.0×10^{-4} M). (b) Naked eye color of **RB-Fe₃O₄@SiO₂** in aqueous solution in presence of various metal ions.

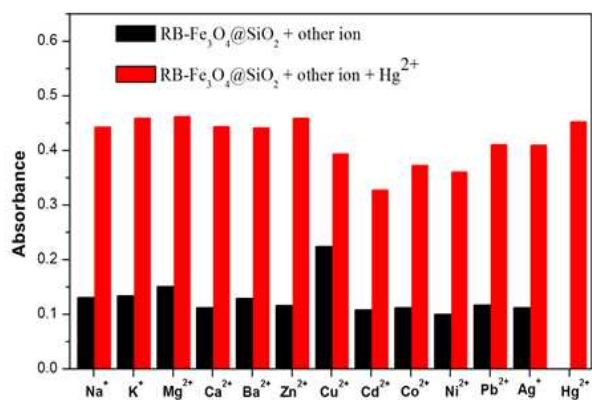


Fig. 8. The absorption spectra of **RB-Fe₃O₄@SiO₂** (0.3 mg/mL) in the presence of various interfering ions (6.0×10^{-4} M), and coexistence with Hg^{2+} ions (6.0×10^{-4} M) in aqueous solution, $\lambda_{\text{abs}} = 570$ nm.

3.3 Fluorescence spectroscopy studies

In order to research the interaction of **RB-Fe₃O₄@SiO₂** with Hg^{2+} , the fluorescence spectra of **RB-Fe₃O₄@SiO₂** for Hg^{2+} in aqueous solution was explored. As shown in Fig. 9, in absence of Hg^{2+} ions, the fluorescence intensity of **RB-Fe₃O₄@SiO₂** is very weak. Under the addition of increasing concentration of Hg^{2+} to the aqueous solution of the suspended **RB-Fe₃O₄@SiO₂** (0.3 mg/mL), a new emission peak near 582 nm could be appeared following the excitation at 535 nm and the fluorescence intensity was gradually enhanced, which could be attributed to the structural transformation from the close spiro lactam structure to the open ring structure upon Hg^{2+} binding⁶⁶. We also determined the linear relationship by plotting the emission intensity of **RB-Fe₃O₄@SiO₂** at 582 nm

as a function of Hg^{2+} ions concentration over a range of $0-7 \times 10^{-5}$ M with a correlation coefficient of 0.99047 (Fig. 10). Based on $3\sigma/k$ (where σ is the standard deviation of the blank measurement, k is the slope of the calibration plot), the limit of detection for Hg^{2+} was up to 2.13×10^{-6} M in aqueous solution.

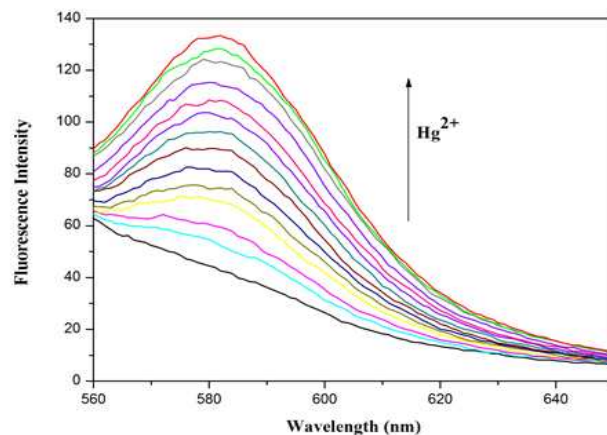


Fig. 9. Fluorescence spectra of **RB-Fe₃O₄@SiO₂** (0.3 mg/mL) in aqueous solution upon addition of various amounts of Hg^{2+} ($0-2.4 \times 10^{-4}$ M) ($\lambda_{\text{ex}} = 535$ nm).

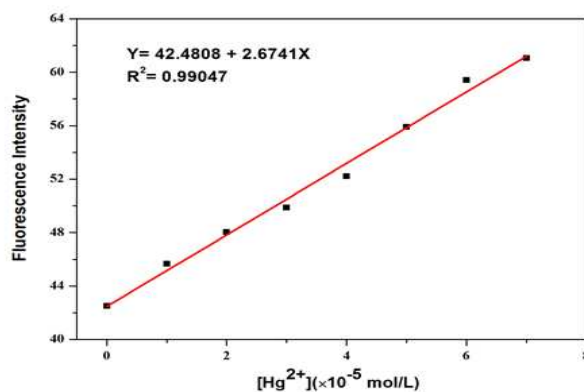


Fig. 10. Fluorescence intensity at 582 nm of **RB-Fe₃O₄@SiO₂** (0.3 mg/mL) in aqueous solution as a function of Hg^{2+} concentration in 10^{-5} M range (0 to 7×10^{-5} M), $\lambda_{\text{ex}} = 535$ nm.

The effect of pH on the fluorescence spectra responses of free **RB-Fe₃O₄@SiO₂** were evaluated (Fig. S5). The results revealed the aqueous solution of the suspended **RB-Fe₃O₄@SiO₂** was non-fluorescent between pH 4 and 10. However, this solution exhibited a strong fluorescence emission band at 582 nm when the pH value was lower than 4 and enhanced with a decrease of the solution pH, which suggested the ring-opening of **RB-Fe₃O₄@SiO₂** because the acyclic structure of rhodamine B derivatives has a strong fluorescence around 580 nm. Thus, the pH range of 4-10 is suitable for using **RB-Fe₃O₄@SiO₂** for the recognition of Hg^{2+} ions.

To further evaluate the selectivity of **RB-Fe₃O₄@SiO₂**, other biologically and environmentally relevant cation species, such as Na^+ , K^+ , Ba^{2+} , Mg^{2+} , Ca^{2+} , Zn^{2+} , Cd^{2+} , Cu^{2+} , Co^{2+} , Ni^{2+} , Pb^{2+} , and Ag^+ ions, were used as the competitive metal ions, at the concentration of 6×10^{-4} M, to examine the selectivity of the sensing probe **RB-Fe₃O₄@SiO₂** toward Hg^{2+}

(2.4×10^{-4} M). It was seen from Fig. 11 that both alkali and alkaline earth metal ions (Na^+ , K^+ , Mg^{2+} , Ca^{2+} , Ba^{2+}), and transition metal ions (Zn^{2+} , Cd^{2+} , Cu^{2+} , Co^{2+} , Ni^{2+} , Pb^{2+} , and Ag^+) have negligible fluorescence changes. However, the addition of Hg^{2+} resulted in a dramatic enhancement of the fluorescence emission intensity positioned around 582 nm. All the above results indicated that **RB-Fe₃O₄@SiO₂** showed a high selectivity toward Hg^{2+} ions.

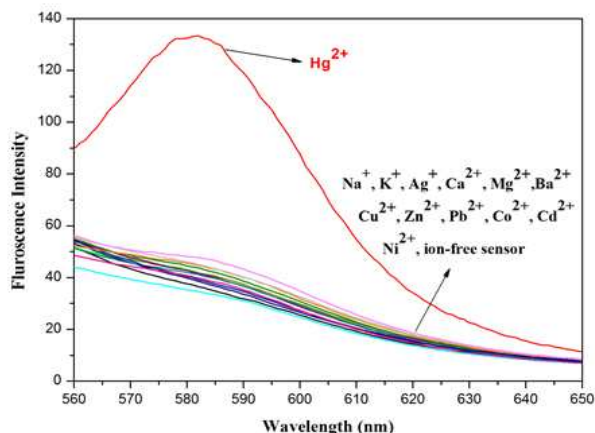


Fig. 11. Fluorescence spectra of **RB-Fe₃O₄@SiO₂** (0.3 mg/mL) in the presence of different metal ions in aqueous solution. $\lambda_{\text{ex}} = 535$ nm, $[\text{Hg}^{2+}] = 2.4 \times 10^{-4}$ M, $[\text{M}^{n+}] = 6 \times 10^{-4}$ M.

Furthermore, the possible influences by other cations were assessed via the competitive experiments. The fluorescence changes of **RB-Fe₃O₄@SiO₂** in aqueous solution were measured by the treatment of Hg^{2+} (2.4×10^{-4} M) in the presence of other competitive metal ions including Na^+ , K^+ , Ba^{2+} , Mg^{2+} , Ca^{2+} , Zn^{2+} , Cd^{2+} , Cu^{2+} , Co^{2+} , Ni^{2+} , Pb^{2+} , and Ag^+ ions (all are 6×10^{-4} M). As shown in Fig. 12, the tested background metal ions showed small or no obvious interference in the Hg^{2+} detection. Thus, the **RB-Fe₃O₄@SiO₂** showed high selectivity toward Hg^{2+} ions, which makes the practical application of **RB-Fe₃O₄@SiO₂** wide and feasible.

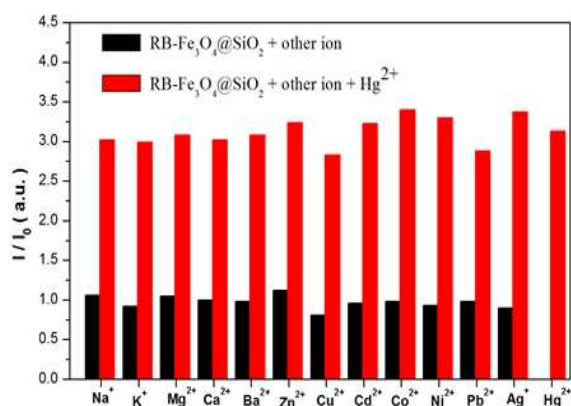
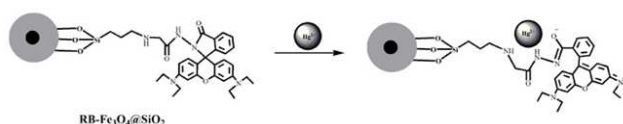


Fig. 12. Fluorescence intensity of **RB-Fe₃O₄@SiO₂** (0.3 mg/mL) in the presence of various interfering ions (6.0×10^{-4} M), and coexistence with Hg^{2+} ions (2.4×10^{-4} M) in aqueous solution, $\lambda_{\text{ex}} = 535$ nm, $\lambda_{\text{em}} = 582$ nm.

3.4 Hg^{2+} ions possible sensing mechanism

In present work, the spirolactam unit of the rhodamine moiety of **RB-Fe₃O₄@SiO₂** serves as a signal switcher, which is expected to turn on when the Hg^{2+} is binded (scheme 2). When the sensing probe **RB-Fe₃O₄@SiO₂** meets Hg^{2+} ions, a Hg^{2+} -promoted ring-opened amide structure is formed, the **RB-Fe₃O₄@SiO₂-Hg²⁺** system forms a conjugated structure, which can serve as the foundation for the sensor for Hg^{2+} .⁶⁶ Furthermore, the chemosensor possibly chelates metal ion via the amide nitrogen like other reported probes.^{14, 38, 67, 68}

To confirm why the obvious absorbance and fluorescence of **RB-Fe₃O₄@SiO₂** changed, the Fourier transform infrared (FT-IR) spectrum of **RB-Fe₃O₄@SiO₂** was recorded in the absence and presence of Hg^{2+} ions (Fig. 13). The peak at 1725 cm^{-1} , which corresponds to the characteristic spirolactam amide carbonyl (C=O) absorption of **RB-Fe₃O₄@SiO₂**, was shifted to the lower frequency (near 1641.2 cm^{-1}) upon binding with Hg^{2+} . This confirmed the notion that the spirolactam amide carbonyl oxygen of **RB-Fe₃O₄@SiO₂** is participated in the coordination of Hg^{2+} .⁶⁹ Moreover, the FT-IR spectra of **RB-Fe₃O₄@SiO₂-Hg²⁺** also showed a shift of N–N frequency from 1548.1 to 1543.5 cm^{-1} , which might be attributed to the binding of Hg^{2+} with the nitrogen of amide group. Hence, according to the above results, the possible binding mechanism between **RB-Fe₃O₄@SiO₂** and Hg^{2+} was proposed in scheme 2.



Scheme 2. The possible sensing mechanism between the **RB-Fe₃O₄@SiO₂** and Hg^{2+} .

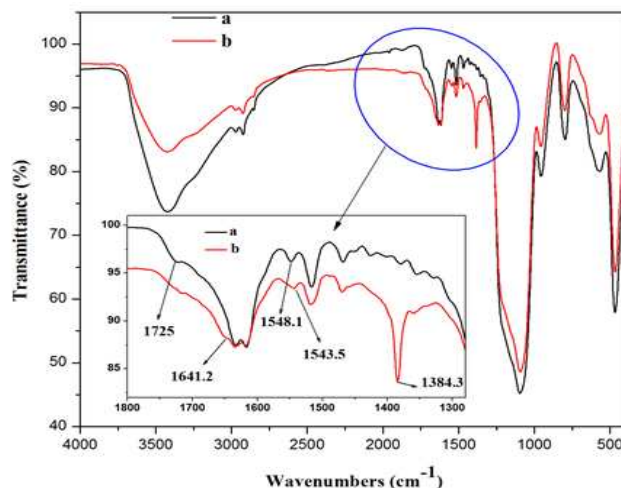


Fig. 13. Comparison between the FT-IR spectral data for **RB-Fe₃O₄@SiO₂** (a) and its metal ion complex **RB-Fe₃O₄@SiO₂-Hg²⁺** (b).

3.5 Preliminary practical application

A preliminary investigation on the utilization of **RB-Fe₃O₄@SiO₂** as a practical absorbent material for Hg^{2+} from the solid-liquid phase solution was carried out for the potential application. A Hg^{2+} solution of about 1×10^{-3} M (10 mL) is treated with 10 mg of **RB-Fe₃O₄@SiO₂** for 12 h. After adding

an external magnetic field, the Hg^{2+} loaded on the nanospheres was isolated from the aqueous solution. Then, inductively coupled plasma spectrometer (ICP-OES) was used to detect the concentration of residual Hg^{2+} in the solution. As shown in Fig. 14, most of the Hg^{2+} was absorbed by the hybrid nanoparticles and only 1.16×10^{-4} M Hg^{2+} remained in the aqueous solution. The measurement results suggested that less than 11.6% of the original Hg^{2+} ions remained in aqueous solution. The result indicates that **RB-Fe₃O₄@SiO₂** can be used as a potential absorbent for efficient removal of Hg^{2+} and has potential practical applications.

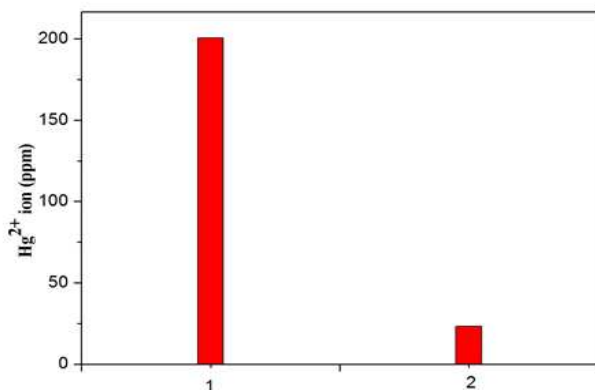


Fig. 14 Adsorption of Hg^{2+} on **RB-Fe₃O₄@SiO₂** surface: concentration of Hg^{2+} before (1) and (2) **RB-Fe₃O₄@SiO₂** treatment. The initial concentration of Hg^{2+} is 1 mM, the volume of Hg^{2+} is 10 mL, the weight of nanoparticles is 10 mg, the adsorption time is 12 h, and the temperature is 25 °C.

4. Conclusions

In conclusion, a novel functional magnetic core-shell nanomaterial is prepared and constructed by covalent coupling of the rhodamine-based receptor RB-Si to the water-soluble magnetic $\text{Fe}_3\text{O}_4@\text{SiO}_2$ nanoparticles. **RB-Fe₃O₄@SiO₂** recognizes Hg^{2+} ions with an excellent selectivity and sensitive optical responses in aqueous solution with a detection limit of 2.13×10^{-6} M. Moreover, it also can efficiently remove Hg^{2+} from aqueous solution and be simply separated from the mixture solution by adding an external magnetic field. These results suggest that **RB-Fe₃O₄@SiO₂** nanocomposite is an excellent alternative for the simultaneous detection and removal of Hg^{2+} in solid liquid phase solution. We believe that inorganic-organic hybrid nanomaterial can play a vital role in the development of the detection and removal of a new generation of toxic metal ions.

Acknowledgements

We wish to acknowledge the institute of coordination chemistry and functional materials of Lanzhou University for providing the instruments of optical measurements.

Notes and references

^a College of Chemistry and Chemical Engineering, Lanzhou University, Lanzhou 730000, PR China.

^b Address here.

^c Address here.

* Please direct correspondence to yansq@lzu.edu.cn. Tel. /fax: +86 931 8912582.

Electronic Supplementary Information (ESI) available: [details of any supplementary information available should be included here]. See DOI: 10.1039/b000000x/

1. T. Y. Cheng, Y. F. Xu, S. Y. Zhang, W. P. Zhu, X. H. Qian and L. P. Duan, *J. Am. Chem. Soc.*, 2008, **130**, 16160-16161.
2. C. Kar, M. D. Adhikari, A. Ramesh and G. Das, *Inorg. Chem.*, 2013, **52**, 743-752.
3. J. Y. Kwon, Y. J. Jang, Y. J. Lee, K. M. Kim, M. S. Seo, W. Nam and J. Yoon, *J. Am. Chem. Soc.*, 2005, **127**, 10107-10111.
4. Q. T. Meng, X. L. Zhang, C. He, G. J. He, P. Zhou and C. Y. Duan, *Adv. Funct. Mater.*, 2010, **20**, 1903-1909.
5. Y. K. Yang, K. J. Yook and J. Tae, *J. Am. Chem. Soc.*, 2005, **127**, 16760-16761.
6. T. W. Clarkson and L. Magos, *Crit. Rev. Toxicol.*, 2006, **36**, 609-662.
7. P. Grandjean, P. Weihe, R. F. White and F. Debes, *Environ. Res.*, 1998, **77**, 165-172.
8. H. H. Harris, I. J. Pickering and G. N. George, *Science*, 2003, **301**, 1203-1203.
9. V. Iyengar and J. Woittiez, *Clin. Chem.*, 1988, **34**, 474-481.
10. W. B. Li, Y. Y. Guo, K. McGill and P. Zhang, *New. J. Chem.*, 2010, **34**, 1148-1152.
11. J. B. Chen, H. Hintelmann and B. Dimock, *J. Anal. Atom. Spectrom.*, 2010, **25**, 1402-1409.
12. A. T. Townsend, K. A. Miller, S. McLean and S. Aldous, *J. Anal. Atom. Spectrom.*, 1998, **13**, 1213-1219.
13. Y. Fu, Q. C. Feng, X. J. Jiang, H. Xu, M. Li and S. Q. Zang, *Dalton Trans.*, 2014, **43**, 5815-5822.
14. J. Jiang, H. E. Jiang, X. L. Tang, L. Z. Yang, W. Dou, W. S. Liu, R. Fang and W. Liu, *Dalton Trans.*, 2011, **40**, 6367-6370.
15. Z. P. Dong, X. Tian, Y. Z. Chen, J. R. Hou, Y. P. Guo, J. Sun and J. T. Ma, *Dyes Pigm.*, 2013, **97**, 324-329.
16. C. Nunez, M. Diniz, A. A. Dos Santos, J. L. Capelo and C. Lodeiro, *Dyes Pigm.*, 2014, **101**, 156-163.
17. S. Lee, B. A. Rao and Y. A. Son, *Sens. Actuators, B*, 2014, **196**, 388-397.
18. S. Mandal, A. Banerjee, S. Lohar, A. Chattopadhyay, B. Sarkar, S. K. Mukhopadhyay, A. Sahana and D. Das, *J. Hazard. Mater.*, 2013, **261**, 198-205.
19. J. K. Ni, Q. Y. Li, B. Li and L. M. Zhang, *Sens. Actuators, B*, 2013, **186**, 278-285.
20. F. Wang, S. W. Nam, Z. Guo, S. Park and J. Yoon, *Sens. Actuators, B*, 2012, **161**, 948-953.
21. D. Zhang, M. Li, M. Wang, J. H. Wang, X. Yang, Y. Ye and Y. F. Zhao, *Sens. Actuators, B*, 2013, **177**, 997-1002.
22. J. F. Zhang and J. S. Kim, *Anal. Sci.*, 2009, **25**, 1271-1281.
23. X. L. Chen, X. M. Meng, S. X. Wang, Y. L. Cai, Y. F. Wu, Y. Feng, M. Z. Zhu and Q. X. Guo, *Dalton Trans.*, 2013, **42**, 14819-14825.
24. W. Huang, D. Y. Wu, G. H. Wua and Z. Q. Wang, *Dalton Trans.*, 2012, **41**, 2620-2625.
25. C. Kaewtong, B. Wannoo, Y. Uppa, N. Morakot, B. Pulpoka and T. Tuntulani, *Dalton Trans.*, 2011, **40**, 12578-12583.

ARTICLE

26. Q. T. Meng, C. He, W. P. Su, X. L. Zhang and C. Y. Duan, *Sens. Actuators, B*, 2012, **174**, 312-317.
27. J. H. Soh, K. M. K. Swamy, S. K. Kim, S. Kim, S. H. Lee and J. Yoon, *Tetrahedron Lett.*, 2007, **48**, 5966-5969.
28. D. Y. Wu, W. Huang, C. Y. Duan, Z. H. Lin and Q. J. Meng, *Inorg. Chem.*, 2007, **46**, 1538-1540.
29. S. H. Kim, K. C. Song, S. Ahn, Y. S. Kang and S. K. Chang, *Tetrahedron Lett.*, 2006, **47**, 497-500.
30. R. Metivier, I. Leray and B. Valeur, *Chem.-Eur. J.*, 2004, **10**, 4480-4490.
31. S. Y. Moon, N. J. Youn, S. M. Park and S. K. Chang, *J. Org. Chem.*, 2005, **70**, 2394-2397.
32. S. Pandey, A. Azam, S. Pandey and H. M. Chawla, *Org. Biomol. Chem.*, 2009, **7**, 269-279.
33. Y. Yu, L. R. Lin, K. B. Yang, X. Zhong, R. B. Huang and L. S. Zheng, *Talanta*, 2006, **69**, 103-106.
34. X. Q. Chen, T. Pradhan, F. Wang, J. S. Kim and J. Yoon, *Chem. Rev.*, 2012, **112**, 1910-1956.
35. H. N. Kim, M. H. Lee, H. J. Kim, J. S. Kim and J. Yoon, *Chem. Soc. Rev.*, 2008, **37**, 1465-1472.
36. S. Adhikari, A. Ghosh, S. Mandal, A. Sengupta, A. Chattopadhyay, J. S. Matalobos, S. Lohar and D. Das, *Dalton Trans.*, 2014, **43**, 12802-12802.
37. J. H. Huang, Y. F. Xu and X. H. Qian, *Dalton Trans.*, 2014, **43**, 5983-5989.
38. S. Z. Ji, X. M. Meng, W. P. Ye, Y. Feng, H. T. Sheng, Y. L. Cai, J. S. Liu, X. F. Zhu and Q. X. Guo, *Dalton Trans.*, 2014, **43**, 1583-1588.
39. D. Guo, Z. P. Dong, C. Luo, W. Y. Zan, S. Q. Yan and X. J. Yao, *RSC Adv.*, 2014, **4**, 5718-5725.
40. H. J. Sheng, X. M. Meng, W. P. Ye, Y. Feng, H. T. Sheng, X. Wang and Q. X. Guo, *Sens. Actuators, B*, 2014, **195**, 534-539.
41. T. Balaji, S. A. El-Safty, H. Matsunaga, T. Hanaoka and F. Mizukami, *Angew. Chem., Int. Ed.*, 2006, **45**, 7202-7208.
42. M. H. Lee, S. J. Lee, J. H. Jung, H. Lim and J. S. Kim, *Tetrahedron*, 2007, **63**, 12087-12092.
43. S. J. Lee, S. S. Lee, J. Y. Lee and J. H. Jung, *Chem. Mater.*, 2006, **18**, 4713-4715.
44. Y. Jing-po, Y. Jun, L. Han and L. Fei, *Dyes Pigm.*, 2014, **106**, 168-175.
45. K. Sarkar, K. Dhara, M. Nandi, P. Roy, A. Bhaumik and P. Banerjee, *Adv. Funct. Mater.*, 2009, **19**, 223-234.
46. E. Kim, H. E. Kim, S. J. Lee, S. S. Lee, M. L. Seo and J. H. Jung, *Chem. Commun.*, 2008, 3921-3923.
47. R. Metivier, I. Leray, B. Lebeau and B. Valeur, *J. Mater. Chem.*, 2005, **15**, 2965-2973.
48. Z. P. Dong, X. Tian, Y. Z. Chen, J. R. Hou and J. T. Ma, *RSC Adv.*, 2013, **3**, 2227-2233.
49. Q. Zou, L. Zou and H. Tian, *J. Mater. Chem.*, 2011, **21**, 14441-14447.
50. F. Ge, M. M. Li, H. Ye and B. X. Zhao, *J. Hazard. Mater.*, 2012, **211**, 366-372.
51. E. Topoglidis, C. J. Campbell, E. Palomares and J. R. Durrant, *Chem. Commun.*, 2002, 1518-1519.
52. X. Tian, Z. P. Dong, R. Wang and J. T. Ma, *Sens. Actuators, B*, 2013, **183**, 446-453.
53. X. H. Peng, Y. J. Wang, X. L. Tang and W. S. Liu, *Dyes Pigm.*, 2011, **91**, 26-32.
54. Y. J. Wang, X. H. Peng, J. M. Shi, X. L. Tang, J. Jiang and W. S. Liu, *Nanoscale. Res. Lett.*, 2012, **7**, 1-13.
55. X. W. Liu, Q. Y. Hu, Z. Fang, X. J. Zhang and B. B. Zhang, *Langmuir*, 2009, **25**, 3-8.
56. R. J. Qu, M. H. Wang, R. F. Song, C. M. Sun, Y. Zhang, X. Y. Sun, C. N. Ji, C. H. Wang and P. Yin, *J. Chem. Eng. Data.*, 2011, **56**, 1982-1990.
57. Y. S. Lin and C. L. Haynes, *Chem. Mater.*, 2009, **21**, 3979-3986.
58. X. F. Yang, X. Q. Guo and Y. B. Zhao, *Talanta*, 2002, **57**, 883-890.
59. Y. H. Wang, B. Li, L. M. Zhang, L. N. Liu, Q. H. Zuo and P. Li, *New. J. Chem.*, 2010, **34**, 1946-1953.
60. L. L. Wang, B. Li, L. M. Zhang, L. G. Zhang and H. F. Zhao, *Sens. Actuators, B*, 2012, **171**, 946-953.
61. L. Sun, Y. X. Li, M. D. Sun, H. G. Wang, S. F. Xu, C. Q. Zhang and Q. B. Yang, *New. J. Chem.*, 2011, **35**, 2697-2704.
62. T. Arita, Y. Ueda, K. Minami, T. Naka and T. Adschiri, *Ind. Eng. Chem. Res.*, 2010, **49**, 1947-1952.
63. M. Sethi, G. Joung and M. R. Knecht, *Langmuir*, 2009, **25**, 317-325.
64. J. Zhang, D. Li, G. Liu, K. J. Glover and T. B. Liu, *J. Am. Chem. Soc.*, 2009, **131**, 15152-15159.
65. J. H. Wang, S. R. Zheng, Y. Shao, J. L. Liu, Z. Y. Xu and D. Q. Zhu, *J. Colloid. Interf. Sci.*, 2010, **349**, 293-299.
66. X. L. Zhang, Y. Xiao and X. H. Qian, *Angew. Chem., Int. Ed.*, 2008, **47**, 8025-8029.
67. Z. P. Liu, C. L. Zhang, X. Q. Wang, W. J. He and Z. J. Guo, *Org. Lett.*, 2012, **14**, 4378-4381.
68. H. Zhu, J. L. Fan, J. Lu, M. M. Hu, J. F. Cao, J. Wang, H. L. Li, X. J. Liu and X. J. Peng, *Talanta*, 2012, **93**, 55-61.
69. M. Wang, F. Y. Yan, Y. Zou, L. Chen, N. Yang and X. G. Zhou, *Sens. Actuators, B*, 2014, **192**, 512-521.